Proceedings for the Symposium on Advanced Research in Energy Technology 2000, Hokkaido University, March 15, 16 and 17, 2000, pp. 95-106.

Experimental Confirmation of the Nuclear Reaction at Low Energy Caused by Electrolysis in the Electrolyte

Tadahiko Mizuno

Section 1. Confirmation with a palladium electrode in the heavy water electrolyte.

1.1 Summary

Many elements on Pd electrodes were confirmed by several analytic methods; reaction products with the mass number up to 208 are deposited on palladium cathodes, which were subjected to electrolysis in a heavy water solution at high pressure, temperature, and current density for prolonged time. These masses were composed of many elements ranging from hydrogen to lead. Extraordinary changes of their isotopic distributions in the produced elements were observed; these were radically different from the ones found in nature. Essentially the same phenomenon was confirmed eight times with high reproducibility at high cathodic current density, above 0.2 A/cm^2. All the possibilities of contamination had been carefully eliminated by several pretreatments for the sample and electrolysis system. It means that a nuclear reaction had taken place during the electrochemical treatment. To explain the production of radiation-less fission-like foreign elements claimed by several electrolysis experiments with Pd cathodes, a selective channel fission model by low-energy multi-photon excitation and collective deformation is proposed. Channel-dependent fission barriers are calculated based on liquid drop model potentials for about 530 scission channels of 6 Pd isotopes with positive Q-values. Mass-distribution, Z-distribution and unnatural isotopic ratios of fission fragments as stable isotopes by the present theory have shown qualitative agreements with the experiments.

2. Introduction

Many claimed that if nuclear reactions have been induced by electrochemical reaction occurring in solid electrodes, there must be clear evidence such as the evolution of radioisotopes and radiation. Moreover, the evolution rates of the reaction products should be quantitatively explained in terms of the proper nuclear reaction mechanisms, but such a claim could be valid if the reaction mechanism is in agreement with current theories. However, there is no proof that the conventional mechanism holds in these reactions. It is difficult to detect the emission of the radiation and radioisotope if the mechanism is different from the accepted ones. In this work, evidence that suggests the occurrence of some nuclear reactions is presented, as isotopic changed elements in and on the cathode surface. These products have been obtained with a mechanism that had not induced any detectable radiation. The anomalous isotopic distribution of these elements shows that they do not come from contamination. We contend that the reaction mechanism was completely different from the normal nucleus formation process. However, we attempt to explain the process that produced these anomalous products by the mechanism within the framework of the accepted theory.

Mizuno[1)], Miley[2)], Ohmori[3)], Iwamura[4)] and others have reported anomalous production of nonradiative foreign elements (Fe, Cr, Ti, Ca, Cu, Zn, Si and so on) on cathode metals (Pd, for

instance) of heavy-water or light-water electrolysis experiments. The also report anomalous, drastically unnatural isotopic ratios of foreign elements. They conceived a kind of fission phenomenon, but did not know the mechanisms of excitation-to-fission, radiation-less fission-products (FP) and selected FP elements with unnatural isotopic ratios. Particle absorption reactions like Pd + p, Pd + n and Pd + d can not excite Pd isotopes over the lowest fission barriers (around 15MeV as shown in this paper) to induce fission, but can induce radioactive compound nuclei and radiation (beta rays, gamma-rays, neutrons and charged particles) which were not observed in experiments. If there were di-neutron capture, excitation near 15MeV would happen but we know that the di-neutron state with a significant lifetime (more than fs) never exists.

We propose here the possibility of fission by collective deformation of Pd nucleus simultaneously absorbing many low-energy photons (1-100keV, for instance) under the dynamic environment of a Pd-cathode in electrochemical experiments, which may lead to selective channel fission for FP pairs within the lowest fission barrier band. Assuming the multi-photon E1 resonance absorption and collective nucleus deformation, scission-channel dependent fission barrier heights were calculated based on the liquid drop model potentials and fission products were analyzed.

3. Experimental

The experimental details of the sample, cell, electrolysis and the reaction conditions have been described elsewhere [5)]. The sample electrodes were subjected to element detection, after pulling off the Teflon coat and washed by the Mill Q water, by means of energy dispersive X-ray spectroscopy (EDX), Auger electron spectroscopy (AES), secondary ion mass spectroscopy (SIMS) and electron probe microanalyzer (EPMA). Palladium rods used were of high purity metal (99.97% min.) supplied by Tanaka Noble Metals, Ltd. Impurities in the sample were as follows; B: 110, Si: 10, Ca: 9, Cr: 8, Cu: 6. Ti: 5, Ag: 41, Pt: 16 and Au: 23 ppm respectively. Nothing more was detected by atomic absorption spectroscopy. The Pd rod was once evacuated in a 5×10^{-5} Torr of vacuum at 473 K for 6×10^{5} sec. Showa Denko, LTD supplied heavy water. It was 99.75% pure and includes 0.077 micro Ci/dm^3 of tritium. The heavy water was purified once in a quartz glass distiller. Reagent grade lithium hydroxide was obtained from Merck, Ltd. Impurities in the reagent were specified as follows; Li_2CO_3: 2% max, Cl: 0.05%, Pb: 16, Ca: 154, Fe: 13, K: 156 and Na: 135 ppm. Other impurities were below the detectable limit by the atomic absorption analysis. The anode and recombiner catalyst was, respectively, a high purity (99.99%) Pt plate and a Pt mesh. The Pt metal is specified to contain impurities as follows; Rh: 18 ppm, Si, Cr and Pd; 2 ppm, Au, Ag, B, Ca, Cu and Fe; less than one ppm. Other impurities were below the limits of detection.

Electrolysis was performed in a closed cylindrical cell made of stainless steel. The cell had another inner Teflon cell made with 1-mm thick wall and 1 cm thick upper cap; the inner height and diameter are 20cm and 7cm, the volume is 770cm^3. Further details have been described elsewhere[6,7)]. Before the electrolysis experiment, 400 cm^3 of electrolyte was once pre-electrolyzed with other Pt mesh electrodes at 1A and 150 °C for 6×10^{5} s (7days) in the cell with the upper cover closed. Next, the Pt electrode was removed and the Pd rod sample was attached to the terminal. Electrolysis experiments were performed with the current density of 0.2A/cm^2 or total current of 6.6A (33cm$^2 \times 0.2$ A/cm^2), at 105 °C for 2.76×10^{6} s (32days). After the electrolysis, the rod was washed with Mill Q water (MillQ-lab; Japan Millipore LTD.) and covered by a Teflon tube. For analysis, the samples were prepared by cutting the rod at 1cm length and again cut in half diametrically by a diamond cutter. The

sample electrodes were subjected to element detection after pulling off the Teflon coat, washing with the Mill Q water. Detection methods used were energy dispersive X-ray spectroscopy (EDX), Auger electron spectroscopy (AES), secondary ion mass spectroscopy (SIMS) and electron probe microanalyzer (EPMA). EDX measurements were done by 20keV of electron irradiation while varying the scanning area; and the energy spectra were measured by Silicon Li drift detector. The energy range of analysis was zero to 20keV; the interesting range was divided into 1024 channels of energy width. The resolution power of energy was 150eV at 5.9keV, but practically that was 200eV. Peaks were calibrated using high purity of C, Al, Si, Ti, Cr, Mn, Fe, Co, Zn, Sr, Nb, Mo, Pd, Ag, Sn, Ce, Hf, W, Pt, Au and Pb. AES analyses were performed by ANELVA AAS-200 to obtain the depth distribution of the elements; the ion irradiation energy and the current were 3keV and 2.5A, respectively. EPMA-8705 of Simazu LTD. was used to obtain the element's distribution on the samples. The SIMS measurements were made by means of an IMA-3 of Hitachi Co.; O_2^+ ions were irradiated to the sample at a spot diameter of 100 micrometers square having a primary energy of 12keV and 100 nano Amperes of ion current. Resolution for the mass was m/e=10000. Mass numbers were calibrated by high purity metals of Li, B, C, Al, Si, Ca, Ti, Cr, Mn, Fe, Co, Ni, Cu, Zn, Sr, Nb, Mo, Pd, Ag, Cd, Sn, Ce, Hf, W, Os, Pt, Au and Pb; no isotopic changes over the natural deviations were noted in the calibration measurements. Careful estimations of the abundance of the each element was required because many mass peaks due to molecules, oxides, hydrides and other complex interfere each other. Then we used various analytic methods to obtain precise isotopic abundance. EPMA analysis was used first to estimate the element's distribution on the sample. AES was employed to obtain the depth distribution of certain elements and EDX measurement determined a relative concentration of the various elements. These techniques were used complementarily in the element estimation because all methods could not necessarily be applicable to all of the elements. After that the SIMS measurement was adopted to decide the elements abundance at the certain point of the sample surface.

4. Results

Many elements were deposited on the surface and distributed irregularly; these concentrations varied by samples. The elements that have commonly been detected on all the samples were C, O, S, Cl, Si, Ca, Ti, Cr, Mn, Fe, Co, Ni, Cu, Zn, Mo, Pd, Sn, Pt, Hg and Pb. The amounts of Ca, Ti, Cr, Cu, Pt, Hg and Pb were abundant and differed by a factor of more than 3 at the surface location as compared with C, Cl, Si, Mn, Co, Ni, Zn and Sn which existed rather uniformly. These changeable elements also fluctuated with sample lots as three times deviations. It may mean that uncontrollable factors such as surface conditions played an important role in the reaction.

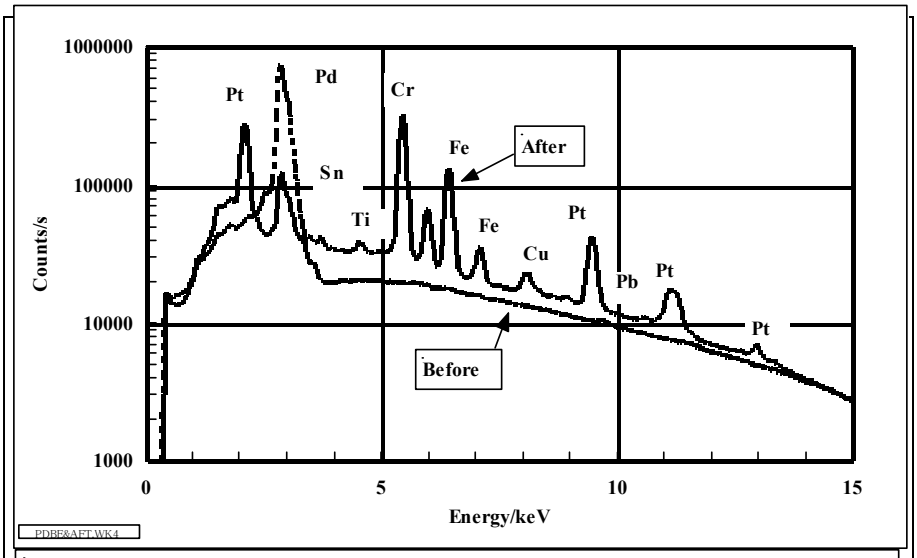

Fig.1 EDX spectra of the Pd rod before and after the electrolysis

Several elements were detected in the Pd electrode by the EDX method; the measurements were taken to determine the rough level of concentration of the elements because mass peaks in the SIMS measurement may contain signals of other molecular peaks. Figure 1 shows typical results before and after the electrolysis. Several peaks of Pt, Cr and Fe are clearly seen. These amounts were comparable with the Pd bulk peak. Less amounts of Sn, Ti, Cu and Pb elements were also clearly observed. The EDX analyses were repeated on various locations on the sample; the deviation of the EDX counts sometimes varied by a factor of 10 depending on the location. This change depended on the scanning area. The amounts of the evolved elements were finally estimated by SIMS measurement. The EDX, AES and EPMA methods were complimentarily used to attribute mass spectra to a certain atom and determine their isotopic distributions. The procedure is described as follows: [1]; the mass number were determined first from light to heavy mass number. [2]; the mass numbers were confirmed referring to the EDX and AES spectra. [3] The large number of mass peaks was used to confirm the existence of their molecular ion and oxide ion peaks. [4] The final mass spectra were estimated by multiplying the factors of counting correction to the original count of mass. The factors took very high and low values for the inert gases and alkali metals respectively.

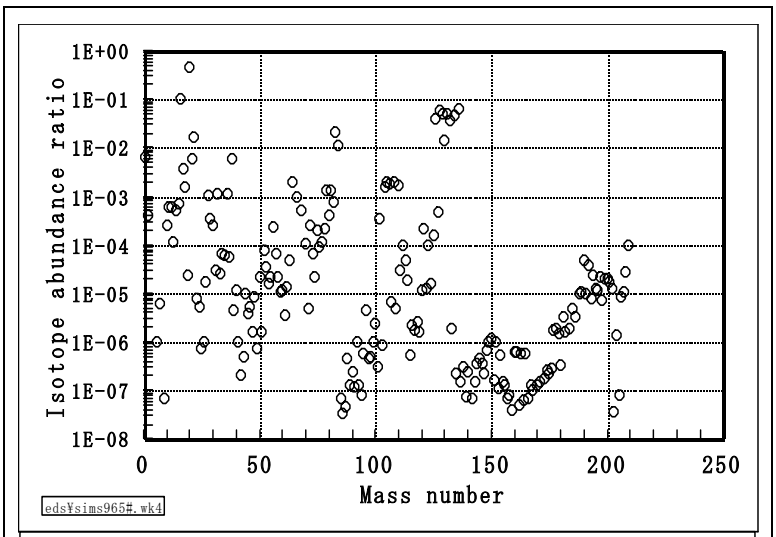

Fig.2 SIMS counting of Pd electrode.

The existing ratios of atomic numbers for the mass were finally estimated with accepted procedures. The ratios are shown in fig.2 after normalizing the total mass as one. Typical counts by EDX and SIMS ranged from 10^2 to 10^6 and were 10 to 100 times higher than the background counts. Thus, the presence of Ca, Ti, Cr, Mn, Fe, Co, Cu, Zn, Cd, Sn, Pt and Pb was clearly confirmed. These elements are mostly grouped in four ranges of mass number: lightest elements under 50, light elements from 50 to 80; middle elements 100 to 140; and heavy elements from 180 to 208. The ratio of the mass number from 102 to 110 which correspond to Pd atom is under 1% of the total even though it was the bulk substance. The large ratio of Oxygen and Xenon pulled down their values. The reason for these

high ratios could be that a large portion of the gas atoms may be released, and contribute to the counting rate, from the spot location where it is heated by ion bombardment.

The SIMS analysis showed other elements; As, Ga, Sb, Te, I, Hf, Re, Ir, Br and Xe. These elements, except for Xe, were difficult to detect by AES and EDX because the peaks were very close and sometime overlapped with others and these were lower than the detection limits of the measurements. Xe atoms are naturally difficult to detect by the EDX method because such gas atoms easily escape from the spot location due to ion bombardment. The SIMS count numbers were observed in the range from 10^3 to 10^6 where the background counts were as low as ~10, so we are confident in these results. In Figure 2 we show the peak intensities normalized on a log scale with the total peak. The intensity of Xe was 10 times larger than Pd; it may be that the gas was released by bombarding with O_2 ions, which caused a temperature rise at the sample. We have observed no peaks except for Pd on the Pd surface after pre-electrolysis. Pt and Pd concentrations in the electrolyte after experiment were 10 and 15 ppm, respectively, as determined by atomic absorption measurement and no other elements except for Li was observed. The total amount of the elements that existed within one micrometer depth of Pd surface were calculated as follows; C: 0.40, O: 8.84, Si: 0.15, S: 0.17, Cl: 0.06, Ca: 0.142, Ti: 0.76, Cr: 22.96, Fe: 10.06, Cu: 5.61, Zn: 3.35, Pd: 33.45, Pt: 9.65, Pb: 4.39 and others less than 0.005 atomic percentage. It may be stressed that the total amount of deposited elements on the Pd is much lower than the summation of the impurity in the electrolyte and Pd samples. Here, the total impurities, except for Ca, Cl, Ti and Hg, are less than the deposited amounts; especially, Zn did not exist as the impurity.

Large differences in isotopic distributions compared with the natural distributions were observed by the SIMS method for Cr, Cu, Zn, Xe, Pd and Pt. Typical concentrations and their ratios for Chromium isotopes are shown in Fig.3. For example, the concentrations except for Cr52 decreased exponentially with depth but Cr52 has a peak at 0.5 micrometers and they showed a large shift in isotopic ratios. Thus, we see large deviations of isotopic existence from natural ones in fig.4. That

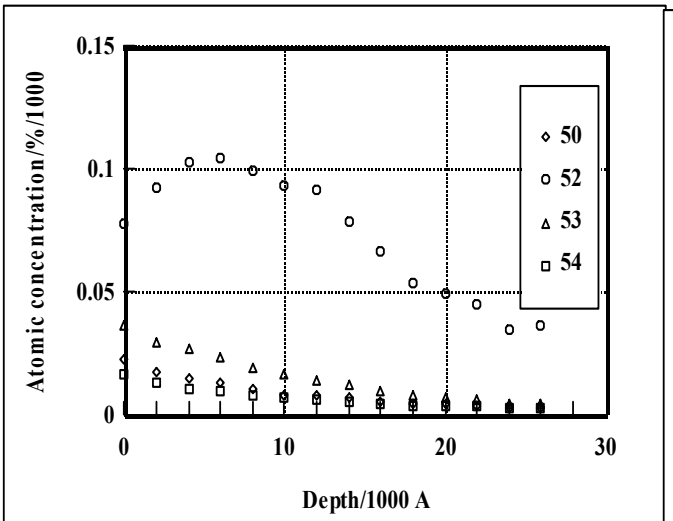

Fig.3 Concentration profiles of Cr isotopes.

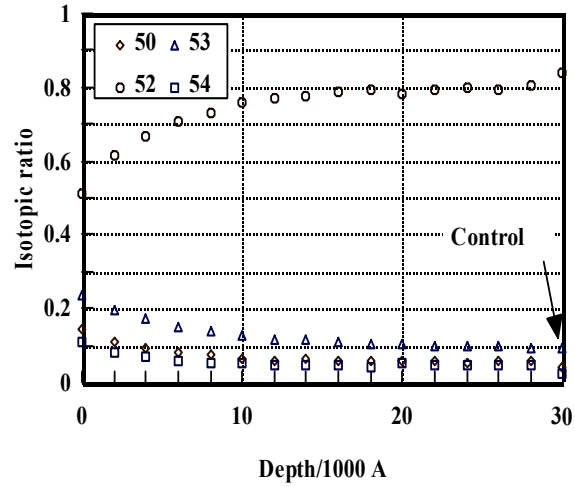

Fig.4 Depth profiles of Cr isotope ratios.

means, Cr52 is less than the others, in the figure where the natural isotopic abundance are plotted at the depth of three micrometers. These isotopic distribution changes occurred mainly within the outer surface layer of one micrometer and their ratios approached normal values toward the inner bulk layer. In fig. 6, Pd also shows large shifts in abundance. Their concentrations are represented with the ratio to Pd106, which is most abundant in the nature. Their atomic concentration increased with depth. This means that the concentration of other deposits have relatively decreased. Especially, amounts of Pd104 and 110 are higher than the natural ones whose values reached normal levels at three micrometers depth in the figure.

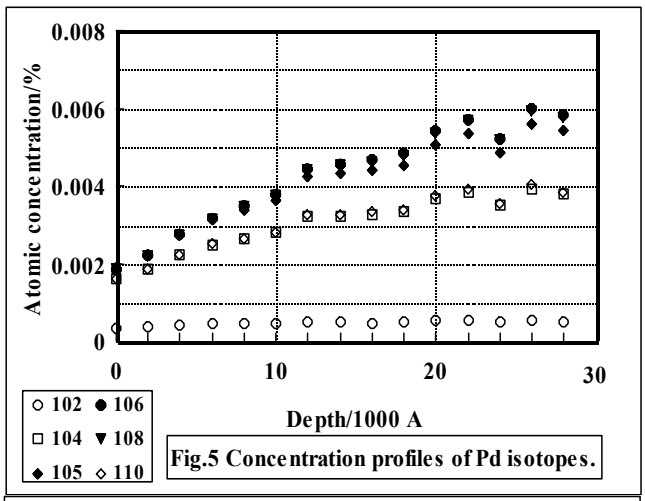

Fig.5 Concentration profiles of Pd isotopes.

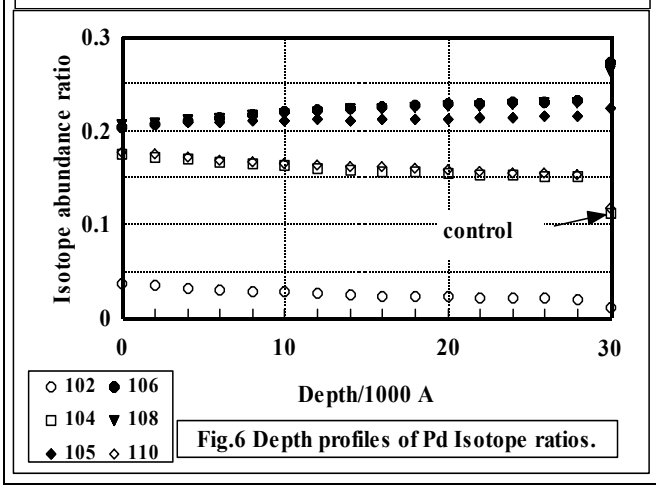

Fig.6 Depth profiles of Pd Isotope ratios.

5. Discussion

Various elements were found to be abundant in the electrolyte and electrode material. Essentially the same phenomenon was confirmed eight times with high reproducibility at high cathodic current density, ranged from 0.2 to 0.8 A/cm^2. It is very unlikely that all of the elements found were impurities in electrolyte, electrode or cell. Even if we suppose that some of the impurities, such as Cr, Fe, Cu and Zn in the system accumulated in the cathode, the amount would be several times smaller than the total amount we detected (Table 1). Different isotope distributions were obtained, depending on the current density and surface treatment. It is simply impossible to explain the shifts in the isotopic distribution. Hence, it must be concluded that some novel reactions have occurred. We assume that the cathode palladium was the starting material for these reactions, but it is also possible that impurities and other cell components such as Li, D_2O, Pd, Pt, K, Na, Ca, B, C, Ag and Fe may have provided the starting material for the nuclear reactions.

5.1 Theoretical model

5.1.1 Possible Photon Sources:

Iwamura[4)] and Fukuoka[9)] have reported the observation of 10-100keV X-ray emission in their Pd/D_2O electrolysis experiments. Taking a hint from these experiments, we assume here that a very high flux of virtual photons with 1-100keV would exist under the dynamic condition of the PdD(H)x lattice or be irradiated on surface of Pd cathode. If we apply the scenario of coherent multi-body deuteron fusion[10)], about 1000 QED-photons (10-100keV) per fusion were generated and one watt

level (10^{11} fusions/s) coherent fusion can produce virtual photon flux of $10^{11} \times 1000 \times 3 \times 10^{10} = 3 \times 10^{24}$ photons/cm^2/s. We assume that this extremely high flux of low-energy photons can induce the multi-photon E1 resonance absorption around 15MeV, by a pumping mechanism via nuclear excitation levels with relatively long life times (nano-sec to micro-sec) of Pd isotopes.

5.1.2 E1 Giant Resonance (EGR) and Fission

The EGR of photonuclear reaction is located in the 15-20 MeV region of photon energy. We assume the single level Breit-Wigner resonance cross section for P-wave with E_r = 15MeV and width Γ = 4MeV. We further assume that the multi-photon EGR can selectively deform Pd nucleus by the collective excitation process: Hence neutron and gamma-ray emission channels are suppressed and the collective deformation of the nucleus is elliptic and then tandem (dumbbell) which may exit to scission events. The scission channel is chaotic because of the existence of so many possible combinations of FP pairs. We consider that deformation for fission is deferent from a scission FP pair to others and therefore each scission channel has its own fission potential with different barrier height (i.e., channel-dependent fission barrier).

5.1.3 Liquid Drop Model

The distortion energy of collective nuclear deformation is given[11)] by

$$\Delta E(r) = [\varepsilon(r)]^2 A^{2/3} \cdot (6.88 - 0.14Z^2/A) \quad \{\text{in fm and MeV units}\} \qquad (1)$$

where, ε (r) is the elliptic deformation coefficient given by

$$\varepsilon(r) = (R_1 + R_2 + r - 2R)/(2R_0) \qquad (2)$$

Using the nuclear radius of Pd R_0, the nuclear radii of FPs R_1 and R_2 and relative distance r of FP_1 and FP_2 nuclei. The point-to-point Coulomb repulsive potential is given as,

$$V_c(r) = 1.44Z_1Z_2/r \quad \{\text{in fm and MeV units}\} \qquad (3)$$

where Z_1 and Z_2 are atomic numbers of FPs.

The first term of Eq.(1) right hand side shows the surface tension of liquid drop and corresponds to the degree of nuclear binding force by strong interaction, and the second term means the change of Coulomb repulsion energy by elliptic distortion. In tandem deformation, scission occurs at $r = R_1 + R_2 + \lambda_\pi$, with the range of strong interaction λ_π (wave length of pion), and at that moment the surface tension vanishes: The effective Coulomb energy E'_c at scission point can be estimated from the difference between $V_c(r)$ and the second term of Eq.(1). We can define the channel dependent fission barrier as,

$$E_{fi} = E'_{ci} - Qi \qquad (4)$$

where Q_i is the Q-value of scission channel i. We have calculated E_{fi} values for about 530 scission channels with positive Q-values, for 6 Pd isotopes (Pd-102, Pd-104, Pd-105, Pd-106, Pd-108 and Pd-110). An example of E_f patterns is shown in Fi.g.1, for Pd-106, where E_f values are plotted as a function of paired two masses of FPs.

5.2 Fission products

5.2.1 Selective Channel Fission

Fission channels with negative Q-values (including neutron and alpha particle emission channels) have such large fission barriers (30 – 50 MeV) that we neglect those for the low-energy photo-fission (LEPF) with an EGR of nuclear excitation energy $E_x > E_r = 15$MeV. With this excitation condition, a limited number of scission channels have smaller fission barriers than E_x as we see in Fig.6, where the lowest fission barrier band (LB1) is the upper line of 11 MeV ($E_r - \Gamma = 15 - 4$) and the lower line of 18 MeV (near $E_r + \Gamma$). For scission channels below $E_f < E_x$, we have estimated tunnel fission probability using the WKB formula[10)] and found that the effect of tunnel fission could not be neglected but remains small. Consequently, we select scission channels with $E_x = E_r$ and $E_x > E_r$ for the first order approximation. Within the LB1 band, there exist 20, 21, 23, 13, 12 and 5 scission channels, respectively for ^{102}Pd, ^{104}Pd, ^{105}Pd, ^{106}Pd, ^{108}Pd and ^{110}Pd. At present, we do not consider the difference in photonuclear excitations of different isotopes of Pd, and simply sum up fission products (FPs) of above 93 channels (SCF channels) within the LB1 band. For 1/3 of SCF channels, we have direct products of stable (nonradiative) FP elements. For the remaining 2/3 of channels, we have stable FP elements after pure beta-decays (about 30 %) and short-lived beta-decays with partial gamma-ray emissions (about 40 %). Only a few channels produce radio-isotopes as final products as ^{60}Fe (1.5×10^6 y: β-decay with 58.59keV γ-ray) and ^{42}Ar(32.9 y: pure β-decay). We list the top 20 channels opening first in Table-1, from which we can extract the following important results: a) 11 channels out of 20 directly produce stable FP elements, b) dominant stable FPs are even Z elements such as Ti, Cr, Fe and Ca, c) naturally abundant isotopes like ^{44}Ca, ^{46}Ca, ^{48}Ca, ^{49}Ti, ^{50}Ti, ^{53}Cr, ^{54}Cr, ^{57}Fe and ^{58}Fe are dominantly produced. Iwamura reported [4)] dominant production of Ca, Ti, Cr and Fe in their D_2O/multi-layered-Pd experiments with EDX and WDX analyses. The LEPF/SCF products of present theory agree very well with his experimental products.

5.2.2 Mass Distribution

The mass distribution of FPs within the LB1 for natural Pd was obtained by summing up isotopic data with weights of natural abundance rates (%) for 6 isotopes and is shown in Fig.7 compared with experimental EPMA data by Mizuno[1)]. The mass distribution curve by the present LEPF/SCF theory has major peaks at A=49, 52 and 56 which respectively correspond to ^{49}Ti, ^{52}Cr and ^{56}Fe, and qualitatively agree well with the Mizuno experiment. The mass distribution of LEPF/SCF for heavier elements (A>180) may have two peaks like uranium fission, for example ^{197}Au is shown elsewhere[11)].

5.2.3 Elements (Z) Distribution

Results are shown in Fig.8, compared with the experimental EDX data by Mizuno[1)]. Stable FP elements for LB1 are distributed from Z = 8 (O) to Z = 40 (Zr). Fe, Cr and Ti are most dominant products, and are followed by Ca, Ni, Zn, Ar, Ge, Mn, V, Si, S, Co, O, Se, Cl, Mg, Sr, Ga, K, Ne, P, Sc, Cu, As, Y and Zr, in the order of yield strength. Qualitative agreement is obtained with Mizuno's experimental data. Theoretical yield strength shows periodical peaks at even Z-values. The effect of nuclear shell structure, especially α-clustered nuclei like ^{16}O, ^{20}Ne, ^{28}Si, ^{48}Ca(double magic nucleus), ^{48}Ti, ^{52}Cr and ^{56}Fe by selective scission channels with low fission barriers will be the explanation to the even-Z effect.

5.2.4 Isotopic Ratios

Detailed data for isotopic production is given elsewhere[7)]. We show only results for 4 major elements. For Ca, ^{40}Ca/^{42}Ca/^{43}Ca/^{44}Ca/^{46}Ca/^{48}Ca ratio by LEPF/SCF-LB1 is 0.0/2.3/12/31.3/20.7/17.3, while the natural abundance ratio is 96.94/0.647/0.135/2.086/0.004/0.187. For Ti, ^{46}Ti/^{47}Ti/^{48}Ti/^{49}Ti/^{50}Ti ratio by LEPF/SCF-LB1 is 1.5/19.6/14.95/33.1/32.0, while the natural abundance ratio is 8.25/7.44/73.72/5.41/5.18. For Cr, ^{50}Cr/^{52}Cr/^{53}Cr/^{54}Cr ratio by LEPF/SCF-LB-1 is 0.3/37.9/31.5/30.3, while the natural abundance ratio is 4.34/83.79/9.5/2.36 and the Mizuno's SIMS data is 3/68/16/13. For Fe, ^{54}Fe/^{56}Fe/^{57}Fe/^{58}Fe ratio by LEPF/SCF-LB1 is 5.98/24.4/30.0/25.8, while the natural abundance ratio is 5.84/91.75/2.12/0.28 and the Iwamura's SIMSdata is 0/45/41/14 compared with the Mizuno's data of 13/64/16/7. We can say that the present theory can qualitatively explain a drastic change of isotopic ratios from natural ones.

6. Conclusions

A fission model of Pd isotopes by the selective channel fission of low-energy multi-photon E1 resonance absorption is proposed and the results of the model calculations have shown significant agreements with experimental foreign element data by electrolyses. The present LEPF/SCF theory can be applied for possible low-energy photo-fission of elements heavier than A=100, and suggests a new method of nuclear-waste transmutation with much less radiation and energy production by largely positive Q-values. Detailed description of the present work will be available elsewhere[11)].

References:

1. Tadahiko Mizuno, et al., Denki Kagaku, Vol.64, No.11 (1996) 1160

2. Gorge Miley, et al., J. New Energy, Vol.1, No.3 (1996) 5

3. Tadayoshi Ohmori, et al., Fusion Technology, 33 (1998) 367

4. Yasuhiro Iwamura, et al., Fusion Technology, 33 (1998) 476

5. Tadahiko Mizuno, et al., "Diffusion Rate of Deuterium in Pd during Cathodic Charging", Denki Kagaku 60, no.5, (1992) 405-411.

6. Tadahiko Mizuno, et al., "Neutron Evolution from Annealed Palladium Cathode in LiOD-D_2O Solution", Denki Kagaku 57, no.7, (1989) 742-743.

7. Tadahiko Mizuno, et al., "Tritium Evolution during Cathodic Polarization of Palladium Electrode in D_2O Solution", Denki Kagaku 59, no.9, (1991) 789-790.

8. H. Fukuoka, et al., Proc. ICCF6, Toya Japan (1996) 425

9. Akito Takahashi, et al., Fusion Technology, 27 (1995) 71

10. Akito Takahashi, et al., Production of Stable Isotopes by Selective Channel Photo-Fission of Pd, submitted to Fusion Technology (April 2000)

Table-1: List of top 20 channels opening first by Pd LEPF

Pd Isotope →	(FP1) +	(FP2) +	(Q MeV)	(Fission Barrier, E_f)
^{104}Pd	^{50}Ti	^{54}Cr	18.96	11.36MeV
^{102}Pd	^{50}Ti	^{52}Cr	18.91	11.60MeV
^{105}Pd	^{51}Ti(5.8min)^{51}V	^{54}Cr	18.24	11.98MeV
^{105}Pd	^{50}Ti	^{55}Cr(3.5min)^{55}Mn	18.12	12.11MeV
^{102}Pd	^{48}Ti	^{54}Cr	17.49	13.03MeV
^{106}Pd	^{48}Ca	^{58}Fe	16.46	13.23MeV
^{106}Pd	^{50}Ti	^{56}Cr(6min)^{56}Mn(2.6h)^{56}Fe	16.81	13.32MeV
^{108}Pd	^{48}Ca	^{60}Fe(1.6x10^{6} y)*	16.10	13.42MeV
^{106}Pd	^{52}Ti(1.7min)^{52}V(3.7min)^{52}Cr	^{54}Cr	16.49	13.63MeV
^{105}Pd	^{47}Ca(4.5d)^{47}Sc(3.3d)^{47}Ti	^{58}Fe	16.07	13.72MeV
^{105}Pd	^{48}Ca	^{57}Fe	15.98	13.81MeV
^{105}Pd	^{52}Ti(1.7min)^{52}V(3.7min)^{52}Cr	^{53}Cr	16.33	13.89MeV
^{104}Pd	^{46}Ca	^{58}Fe	15.89	14.01MeV
^{102}Pd	^{51}V	^{51}V	16.47	14.10MeV
^{102}Pd	^{46}Ca	^{56}Fe	15.81	14.27MeV
^{102}Pd	^{44}Ca	^{58}Fe	15.69	14.42MeV
^{105}Pd	^{46}Ca	^{59}Fe(44d)^{59}Co	15.38	14.43MeV
^{104}Pd	^{48}Ca	^{56}Fe	15.42	14.45MeV
^{110}Pd	^{48}Ca	^{62}Fe(1.1min)^{62}Co(14min)^{62}Ni	14.76	14.59MeV
^{102}Pd	^{49}Ti	^{53}Cr	15.91	14.60MeV

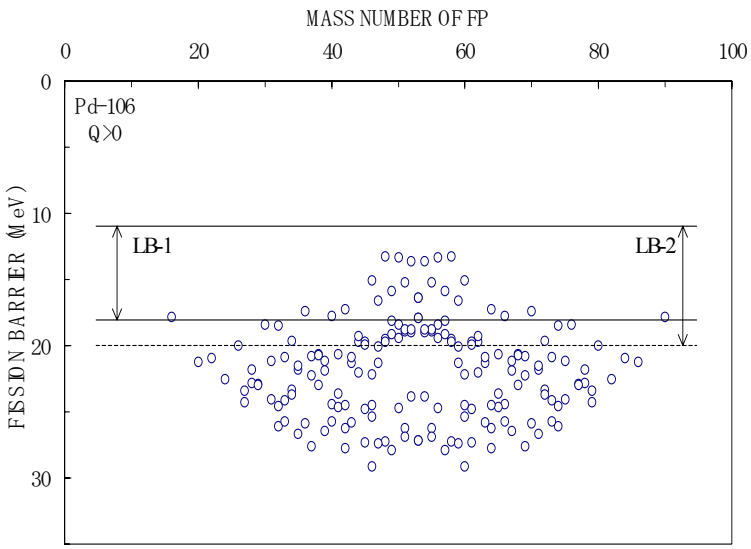

Fig.7: Map of channel-dependent fission barriers for Pd-106

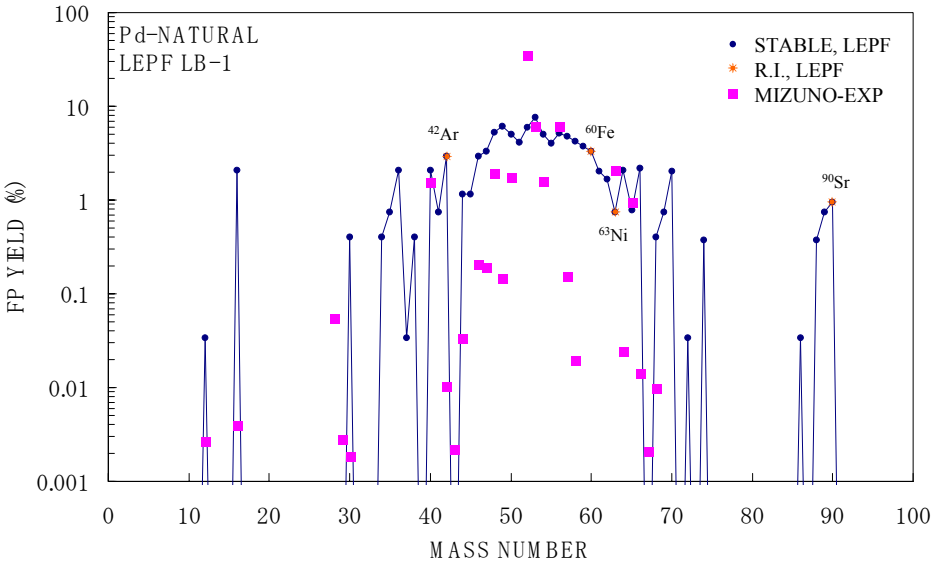

Fig.8: Mass distribution of Pd -LEPF

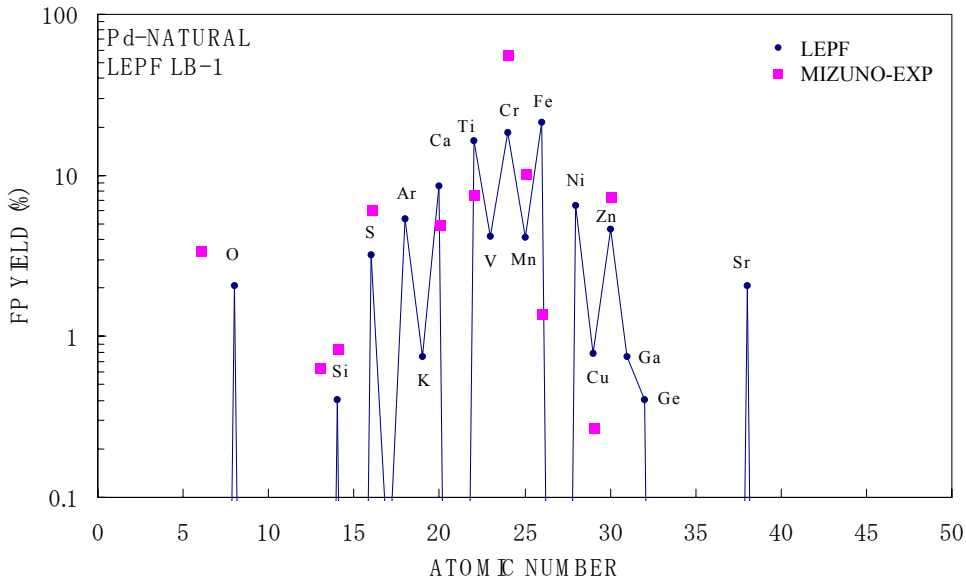

Fig.9: Elements (Z) distribution of Pd -LEPF